Thermodynamic and structural insights into CSL-DNA complexes

David R. Friedmann and Rhett A. Kovall*

Department of Molecular Genetics, Biochemistry and Microbiology, University of Cincinnati College of Medicine, Cincinnati, Ohio 45267-0524

Received 27 July 2009; Revised 19 October 2009; Accepted 20 October 2009
DOI: 10.1002/pro.280
Published online 28 October 2009 proteinscience.org

Abstract: The Notch pathway is an intercellular signaling mechanism that plays important roles in cell fates decisions throughout the developing and adult organism. Extracellular complexation of Notch receptors with ligands ultimately results in changes in gene expression, which is regulated by the nuclear effector of the pathway, CSL (C-promoter binding factor 1 (CBF-1), suppressor of hairless (Su(H)), lin-12 and glp-1 (Lag-1)). CSL is a DNA binding protein that is involved in both repression and activation of transcription from genes that are responsive to Notch signaling. One well-characterized Notch target gene is *hairy and enhancer of split-1* (*HES-1*), which is regulated by a promoter element consisting of two CSL binding sites oriented in a head-to-head arrangement. Although previous studies have identified *in vivo* and consensus binding sites for CSL, and crystal structures of these complexes have been determined, to date, a quantitative description of the energetics that underlie CSL-DNA binding is unknown. Here, we provide a thermodynamic and structural analysis of the interaction between CSL and the two individual sites that comprise the *HES-1* promoter element. Our comprehensive studies that analyze binding as a function of temperature, salt, and pH reveal moderate, but distinct, differences in the affinities of CSL for the two *HES-1* binding sites. Similarly, our structural results indicate that overall CSL binds both DNA sites in a similar manner; however, minor changes are observed in both the conformation of CSL and DNA. Taken together, our results provide a quantitative and biophysical basis for understanding how CSL interacts with DNA sites *in vivo*.

Keywords: Notch signaling; protein-DNA interactions; X-ray crystallography; isothermal titration calorimetry; thermodynamics

Introduction

Notch signaling is an evolutionarily conserved cell-to-cell signaling pathway in metazoans that has indispensable roles during embryonic development and postnatal tissue homeostasis, such as during organogenesis and lymphopoesis, respectively.[1,2] Improper signaling results in congenital defects, cardiovascular disorders, and cancer.[3–5] Signaling is initiated when the ligand, termed DSL (Delta, Serrate, Lag-2), on the surface of one cell binds to the extracellular region of the receptor Notch on a neighboring cell.[6] This interaction results in two proteolytic cleavage events of Notch, culminating in the release of the intracellular domain of the Notch receptor (NotchIC) from the membrane and translocation of NotchIC to the nucleus. Once inside the nucleus, NotchIC binds the transcription factor CSL (CBF-1, Su(H), Lag-1), which results in recruitment of the transcriptional coactivator Mastermind and conversion of CSL from a repressor to an activator of transcription from Notch responsive genes.[7]

Previous studies of CSL orthologs from *Homo sapiens* (CBF-1), *Mus musculus* (RS-binding protein (RBP)-Jκ), *Drosophila melanogaster* (Su(H)), and

Additional Supporting Information may be found in the online version of this article.

Grant sponsor: Fellowship from the American Heart Association (to D.R.F.); Grant sponsor: National Institutes of Health; Grant number: CA120199 (to R.K.).

*Correspondence to: Rhett A. Kovall, 231 Albert Sabin Way, Cincinnati, OH 45267-0524. E-mail: kovallra@ucmail.uc.edu

Published by Wiley-Blackwell. © 2009 The Protein Society

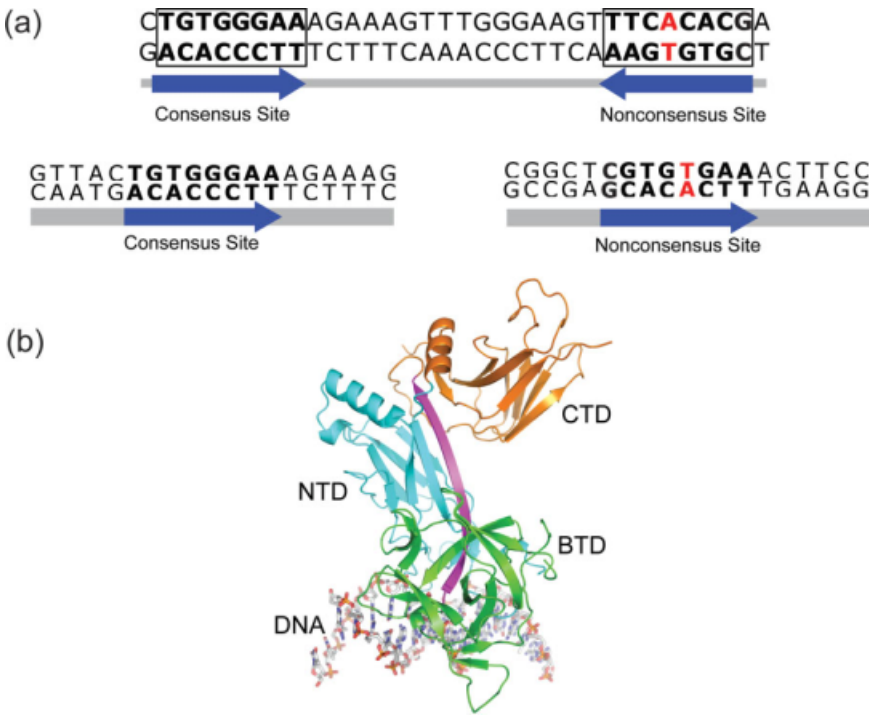

Figure 1. *HES-1* SPS and CSL structure. (A) Nucleotide sequence and schematic representation of the mammalian *HES-1* SPS (top) and the oligomeric DNA duplexes corresponding to the consensus and nonconsensus sites of the *HES-1* SPS (bottom) that were used in the herein described binding studies. CSL-binding sites are in bold text and arrows denote directionality of binding sites. The T/A base pair that deviates from the consensus is colored red. (B) Ribbon diagram for mouse CSL-DNA structure (3BRG). The NTD, BTD, and CTD are colored cyan, green, and orange, respectively. The DNA is in a stick representation with carbon, oxygen, nitrogen, and phosphorous atoms colored grey, red, blue, and orange, respectively. The DNA from this complex structure corresponds to the *HES-1* consensus binding site.

Caenorhabditis elegans (Lag-1) revealed that CSL is a sequence specific DNA binding protein that binds the consensus sequence -C/tGTGGGAA-.[8–11] DNA sequences similar to the consensus have been identified within the promoter regions of Notch target genes in organisms ranging from flies and worms to humans and even in the genomes of the herpesviruses, Epstein-Barr virus and Kaposi's sarcoma-associated herpesvirus.[12–15] However, more complicated arrangements of CSL binding sites have also been observed, for example the enhancer of split gene complex (E(spl)-C) in flies.[12] Certain genes of the E(spl)-C contain a unique promoter architecture, termed Su(H)-paired site (SPS), consisting of two CSL binding sites arranged in a head-to-head manner with an approximately 16 base pair A/T rich spacer sequence [Fig. 1(A)]. The SPS architecture has also been identified in the *hairy and enhancer of split-1* (*HES-1*) genes found in mammals.[16] Interestingly, one of the binding sites of the *HES-1* SPS conforms precisely to the consensus binding site determined for CSL (-TGTGGGAA-), whereas the second site deviates from the consensus (-CGTGTGAA-); that is the T/A base step in the fifth position of the binding site was not observed in one of the consensus binding studies and infrequently observed in the other.[9,8] Moreover, the sequence corresponding to the nonconsensus site for the *HES-1* SPS is conserved in mammals and conserved in some, but not all SPS sites found in *Drosophila*, Zebrafish, and *Xenopus*. -TGTGGGAA- and -CGTGTGAA- sites that comprise the *HES-1* SPS are hereafter referred to as consensus and nonconsensus sites, respectively.

More recently, high resolution crystal structures for CSL-DNA and CSL-coregulator-DNA complexes have been determined by our group, and by Nam *et al.*, for CSL orthologs from worm, mouse, and human [Fig. 1(B)].[17–20] All of these complex structures used oligomeric DNA duplexes that corresponded to the *HES-1* consensus [Fig. 1(A)], and to date, no CSL-DNA structure has been determined using any other known CSL binding site. These structures elucidated the molecular interactions that underlie specific DNA binding by CSL, and overall, despite different bound coregulators, are remarkably similar. The *N*-terminal domain (NTD) and β-trefoil domain (BTD) of CSL cooperate to specifically recognize base pairs in the major and minor grooves, respectively, and form a positively charged surface to make nonspecific interactions with the phosphodiester backbone of DNA. The protein residues involved in DNA binding are absolutely conserved

amongst all CSL orthologs. Moreover, crystal structures of worm and human CSL-NotchIC-Mastermind ternary complexes displayed protein-DNA interactions very similar to CSL-DNA structures, suggesting that the formation of an active transcription complex does not alter how CSL binds to DNA.[21] After the determination of the human CSL-NotchIC-Mastermind ternary complex structure, Nam *et al.*[22] described the cooperative assembly of two ternary complexes on the *HES-1* SPS, in which interactions between the ankyrin repeats of NotchIC mediated the observed cooperativity. Moreover, the cooperative binding was dependent on the orientation and spacing of the two CSL binding sites within the SPS.[22]

Despite these advances in the field, there remains a significant gap in our understanding of the energetics that underlie CSL binding to DNA, and whether any structural or affinity differences arise when CSL binds to DNA sites other than the *HES-1* consensus site. The goal of this study was to address this gap in our understanding by (1) thermodynamically characterizing the binding of CSL to the two individual sites that compose the *HES-1* SPS and (2) determining the X-ray structure for CSL bound to the *HES-1* nonconsensus site. Our isothermal titration calorimetry (ITC) data show moderate differences for the affinity of CSL with the consensus and nonconsensus sites of the HES-1 SPS. A thorough analysis of binding as a function of temperature, salt, and pH allowed us to construct thermodynamic profiles of CSL binding to each individual site, which reveals distinct thermodynamic modes of binding. Our determination of a structure of CSL bound to the *HES-1* nonconsensus site reveals, when compared with previous structures, alternative modes of binding used by CSL to interact with DNA. Taken together, our thermodynamic and structural studies provide for a more thorough understanding of CSL-DNA interactions; data that are essential for developing and interpreting models of cooperative assembly of CSL-mediated transcription complexes binding at the *HES-1* promoter element.

Results

Thermodynamics of CSL-DNA interactions

To address questions regarding the affinity of CSL for DNA, we used ITC to characterize the binding of recombinantly purified murine CSL protein with chemically synthesized oligomeric DNA duplexes that correspond to the consensus and nonconsensus sites of the *HES-1* SPS (Fig. 2). All ITC experiments were performed by titrating the DNA duplex from the syringe into the cell containing CSL. Initial experiments at 25°C displayed little or no measurable heat signal on binding, precluding analysis; however, experiments performed at the following temperatures (5°C, 10°C, and 15°C) allowed for determination of the thermodynamics of CSL-DNA binding. As shown in Table I, CSL binds the consensus and nonconsensus DNA sites with similar energetics. The stoichiometries of the complexes are 1:1 with ~150 and ~300 nM dissociation constants (K_d) observed for CSL binding to the consensus and nonconsensus sites, respectively, that is, a modest 2-fold tighter and ~0.3 kcal/mol greater free energy of binding observed for the consensus DNA across the temperature range tested. Both consensus and nonconsensus binding reactions are endothermic at temperatures between 5°C and 15°C, and as typical for many DNA-binding proteins, the binding reaction is entropically driven.[23] As shown in Figure 3, plotting the thermodynamic data as a function of temperature highlights the enthalpy/entropy compensation that is observed, because the overall free energy of binding (ΔG°) is virtually temperature independent. Again, this binding phenomenon has been observed for other DNA-binding proteins.[24] Figure 3 also illustrates why we were unable to measure binding at 25°C, as the enthalpic contribution to binding approaches zero near 25°C. We were also unable to measure binding at 37°C and 45°C, which we attribute to a lack of measurable heat upon complex formation at these temperatures.

We next determined the change in heat capacity (ΔCp) associated with the binding of CSL to the consensus and nonconsensus DNA sites, by analyzing the enthalpy of binding as a function of temperature (Fig. 3 and S1). It has been suggested that a large and negative ΔCp value associated with a protein-DNA binding reaction correlates with burying a sizeable amount of nonpolar surface area and/or a conformational change upon complex formation.[25–27] The ΔCp values determined from our ITC binding experiments are -0.31 and -0.30 kcal mol^{-1} K^{-1} for CSL interacting with the consensus and nonconsensus DNA sites, respectively. Comparison of the ΔCp values suggests no significant thermodynamic differences in the amount of buried surface area (BSA) or conformational changes for the two complexes.

We attempted to determine the ΔCp of binding based on the amount of BSA calculated from the structures of CSL-DNA complexes; however, as similarly reported by others, we found a large discrepancy between the observed and calculated ΔCp values, regardless of which method we used.[28,29] Our calculated values tended to underestimate the ΔCp of binding by as much as 0.1 kcal mol^{-1} K^{-1}. Because there are no structures of CSL in the absence of DNA, our calculations cannot account for folding of CSL coupled to DNA binding, which may account for the discrepancy in the experimentally determined and calculated values of ΔCp. Interestingly, in a previous study, we observed a 2 kcal/mol enthalpy/entropy compensation for the binding of

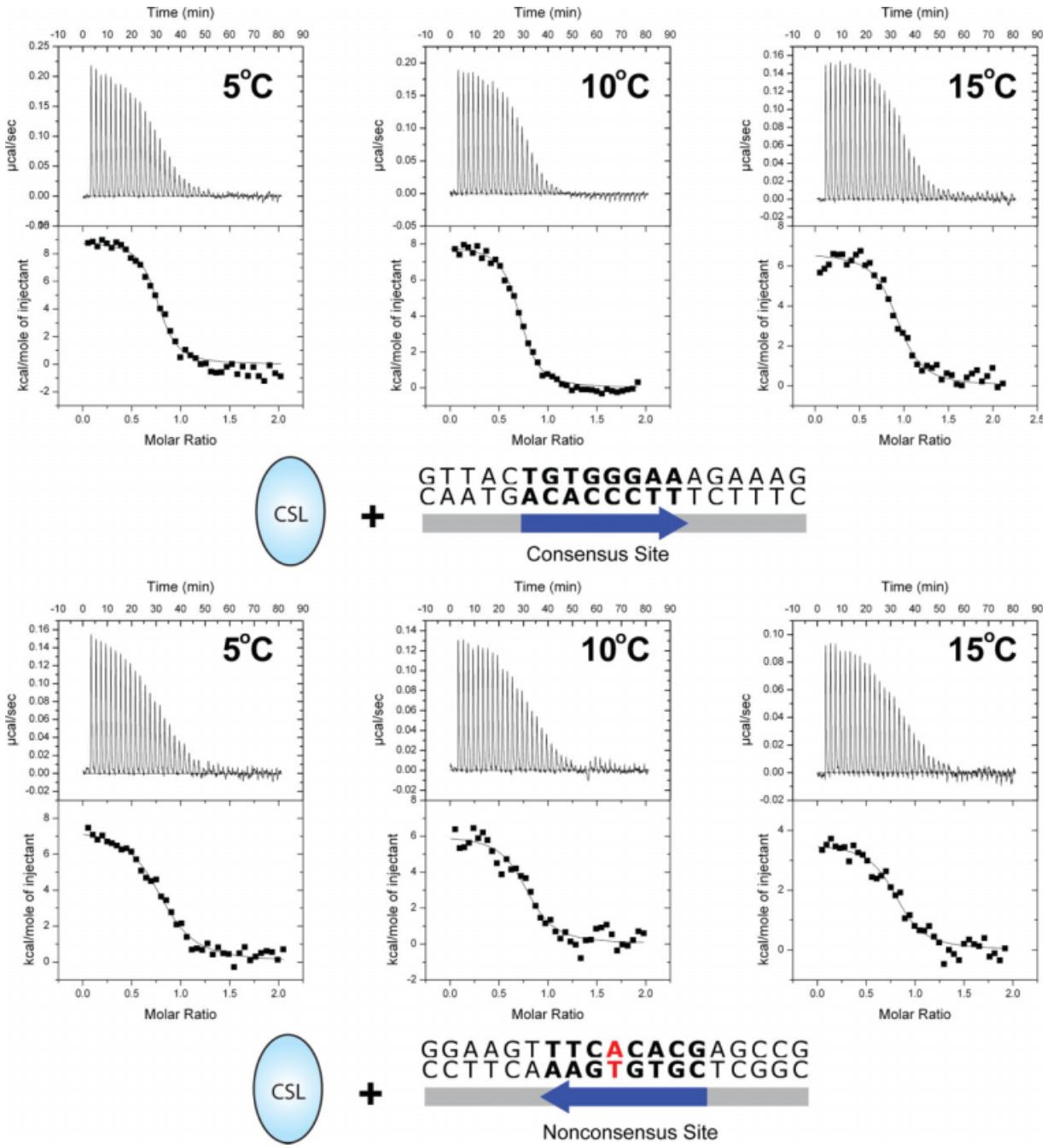

Figure 2. CSL-DNA ITC binding assays. Figure shows representative thermograms (raw heat signal and nonlinear least squares fit to the integrated data) for CSL binding to DNA corresponding to the *HES-1* 5′ consensus site (top) and the 3′ nonconsensus site (bottom). Data were measure at 5°C, 10°C, and 15°C in a phosphate buffer at pH 6.5 with 150 m*M* NaCl. Forty titrations were performed per experiment, consisting of 7-µl injections of DNA that were spaced 120 sec apart. [Color figure can be viewed in the online issue, which is available at www.interscience.wiley.com.]

CSL to the Rbp-j associated molecule (RAM) domain of NotchIC in the presence and absence of DNA, which may suggest that regions of CSL undergo folding coupled to DNA binding.[20]

CSL orthologs binding to DNA

To address whether the affinity of CSL for DNA is conserved, we performed similar ITC experiments using the worm and fly orthologs of CSL, Lag-1, and Su(H), respectively. As shown in Table II, binding of both Lag-1 and Su(H) to DNA is similar to what we observed for our murine CSL binding experiments, that is the affinity of CSL orthologs for the consensus DNA site was approximately 2-fold stronger than binding to the *HES-1* nonconsensus site with K_d values of ~200 and ~400 n*M*, respectively. Moreover, the free energy of binding was similar, approximately −8 kcal/mol. Because of the similarity of

Table I. *Temperature Dependence of CSL Binding to Consensus and Nonconsensus Sites of the HES-1 SPS*

	T (°C)	K (M^{-1})	K_d (nM)	ΔG° (kcal/mol)	ΔH° (kcal/mol)	−TΔS° (kcal/mol)
Consensus	5	7.78 (±0.80) × 10^6	129	−8.76 ± 0.06	9.18 ± 0.31	−17.9 ± 0.3
HES-1 DNA	10	5.05 (±1.54) × 10^6	209	−8.66 ± 0.16	7.69 ± 0.18	−16.3 ± 0.3
	15	5.56 (±0.72) × 10^6	182	−8.88 ± 0.08	6.08 ± 0.54	−14.7 ± 0.5
Nonconsensus	5	3.45 (±0.91) × 10^6	307	−8.30 ± 0.16	6.54 ± 0.80	−14.8 ± 0.6
HES-1 DNA	10	3.97 (±0.14) × 10^6	252	−8.54 ± 0.02	5.67 ± 0.35	−14.2 ± 0.4
	15	3.04 (±0.42) × 10^6	333	−8.54 ± 0.08	3.60 ± 0.05	−11.9 ± 0.04

Consensus DNA, -GTTAC**TGTGGGAA**AGAAAG-; nonconsensus DNA, -CGGCT**CGTGTGAA**ACTTCC-.
Values are the mean of at least three independent experiments, and the errors represent the standard deviation of multiple experiments.

DNA binding observed for the three CSL orthologs (mouse, worm, and fly) and the high degree of sequence identity between orthologs, we conclude that the affinity of CSL for DNA has been highly conserved through evolution, and for the remainder of our analysis, we focused our binding studies exclusively on murine CSL with the *HES-1* consensus and nonconsensus sites.

Effect of salt concentration on DNA binding

To investigate the contribution of ionic interactions to complexes formed between CSL and DNA, we performed a series of ITC binding experiments over a range of NaCl concentrations. As shown in Table III and plotted in Figure 4, the binding of CSL to DNA is sensitive to increasing concentrations of salt, displaying the same trend for both consensus and nonconsensus sites; as the concentration of salt increases, correspondingly the association constant (K) and free energy of binding (ΔG_{obs}) decrease; however, binding displayed a nonlinear dependence on concentrations of salt below 125 mM (Fig. 4). Although the molecular basis for this nonlinearity is outside the scope of this study, it should be mentioned that a similar nonlinear dependence of binding has been observed for the structurally related transcription factor nuclear factor (NF)-kappaB,[30] and for other DNA-binding proteins[31]. A closer examination of the enthalpic and entropic contributions to binding at 150 and 200 mM salt reveals a modest change in the enthalpy of binding (less than 1.0 kcal/mol), but a large entropic penalty of ~3.0 kcal/mol for both reactions. These data demonstrate that increasing the salt concentration affects the entropy of binding to a greater extent than the enthalpy, which has been observed for other DNA-binding proteins, whereby binding is driven by the entropically favorable release of counterions from DNA.[32,33]

Effect of pH on CSL-DNA interaction

To address the influence solution pH has on CSL-DNA complexes and potentially identify any ionizable groups involved in binding, a series of experiments were performed in buffers ranging from pH 6.0 to 8.0 (Table IV and Supporting Information Fig. S2). CSL binding to both consensus and nonconsensus DNA sites is nearly linearly dependent on pH between 6.0 and 8.0, with significantly stronger binding occurring at pH 6.0. Comparison of binding at pH 6.0 and pH 8.0 reveals that there is approximately a 15-fold and 1.5 kcal/mol difference in the association constant and free energy of binding, respectively (Table IV). Although the overall free energies of binding for both the consensus and nonconsensus sites are similar over the pH range, the

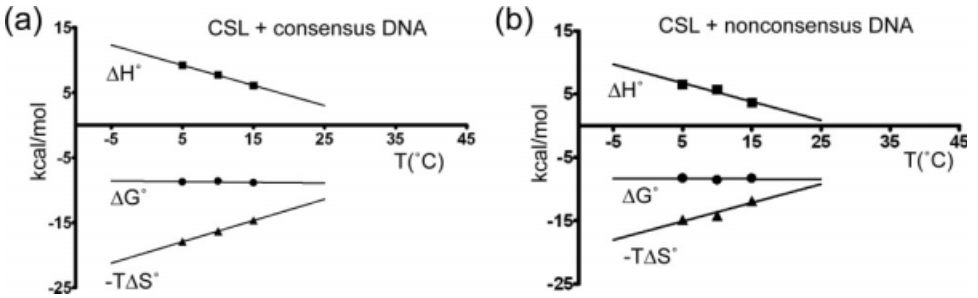

Figure 3. Thermodynamic profiles for CSL binding to the consensus and nonconsensus *HES-1* DNA sites. Figure shows plots of thermodynamic parameters for CSL binding to the consensus site (A) and nonconsensus site (B) that comprise the *HES-1* SPS. A straight line was fit to data collected at 5°C, 10°C, and 15°C, highlighting the compensatory changes in enthalpy (ΔH°) and entropy (−TΔS°) as a function of temperature, which maintain a relatively temperature independent free energy of binding (ΔG°). The heat capacity change (ΔCp) was calculated from the slope of the line fit to the enthalpic data measured at 5°C, 10°C, and 15°C. The ΔCp values for CSL binding to the consensus and nonconsensus sites are −0.31 and −0.30 kcal/mol/K, respectively.

Table II. *CSL Orthologs Binding to DNA*

CSL	DNA	K_{app} (M^{-1})	K_d (nM)	ΔG_{obs} (kcal/mol)	ΔH_{obs} (kcal/mol)	$-T\Delta S_{obs}$ (kcal/mol)
Worm CSL (Lag-1)	*HES-1* consensus	$5.20\ (\pm1.8) \times 10^6$	192	−8.79	6.11 (±0.2)	−15.0
Worm CSL (Lag-1)	*HES-1* nonconsensus	$2.34\ (\pm0.5) \times 10^6$	427	−8.10	6.49 (±0.2)	−14.6
Fly CSL Su(H)	*HES-1* consensus	$4.19\ (\pm0.4) \times 10^6$	239	−8.4	9.6 (±0.1)	−18.0
Fly CSL Su(H)	*HES-1* nonconsensus	$3.49\ (\pm0.4) \times 10^6$	286	−8.3	6.9 (±0.1)	−15.2

All experiments are performed at 5°C.
Consensus DNA, -GTTAC**TGTGGGAA**AGAAAG-; nonconsensus DNA, -CGGCT**CGTGTGAA**ACTTCC-.
The errors represent the standard deviation of the nonlinear least squares fit of the data to the titration curves.

enthalpic and entropic contributions to binding are strikingly different. There is approximately a 3 kcal/mol more favorable enthalpic contribution to binding for CSL complexes formed with the nonconsensus DNA, and conversely, a 3 kcal/mol more favorable entropic contribution to binding for CSL complexes formed with the consensus DNA site. As shown in Supporting Information Figure S2, the slope of the line, resulting from plotting the log of the association constant (K) as a function of pH, reveals the number of ionizable residues that participate in complex formation.[34] The slope of these lines for CSL binding to both consensus and nonconsensus DNA sites, over the pH range tested, is approximately 1 (Supporting Information Fig. S2).

CSL binding other nonconsensus sites

We next sought to address the functional significance of the conserved T/A base step in the 3′ nonconsensus site of the *HES-1* SPS (-CGTG**T**GAA-) by performing ITC binding experiments with DNA duplexes that have either an adenine (-CGTG**A**GAA-) or a cytosine (-CGTG**C**GAA-) base substituted at this position. Experiments performed with the T→A substitution revealed binding affinities and energetics similar to those observed with the *HES-1* consensus DNA site (K_d = ∼150 nM and ΔG_{obs} = −8.6 kcal/mol; Table V). These data are consistent with previous consensus binding site studies for CSL, in which an A/T base step was observed at this position, albeit with considerable lower frequency than a G/C base step.[9,8] However, experiments performed with the T→C substitution revealed a strikingly lower affinity of CSL for this DNA with a K_d of ∼1 μM and ΔG_{obs} = −7.6 kcal/mol (Table V). This represents an approximately 7- and 3-fold difference in affinity when compared with CSL binding to the consensus and nonconsensus sites, respectively, of the *HES-1* SPS.

Structure of murine CSL bound to nonconsensus DNA

To identify any structural differences for CSL binding the nonconsensus site, and potentially identify a structural basis for the differences observed in the thermodynamics of binding, we determined the X-ray structure of murine CSL bound to the nonconsensus site at 2.0 Å resolution. This structure was compared with our previously determined structure of murine CSL bound to the consensus site of the *HES-1* SPS (PDB ID: 3BRG).[20] The CSL-nonconsensus DNA complex crystallizes with similar unit cell dimensions, belongs to the same space group symmetry, and forms comparable crystal lattice contacts as the previously determined CSL-consensus DNA complex. Structural alignment of the Cα atoms for the two structures reveals that overall, the two protein-DNA complexes are similar—408 corresponding Cα atoms overlay with an root mean square

Table III. *Salt Dependence of CSL Binding to Consensus and Nonconsensus HES-1 Sites*

	Salt, NaCl (mM)	K_{app} (M^{-1})	K_d (nM)	ΔG_{obs} (kcal/mol)	ΔH_{obs} (kcal/mol)	$-T\Delta S_{obs}$ (kcal/mol)
Consensus	50	$2.36\ (\pm0.8) \times 10^7$	42	−9.38	8.76 (±0.2)	−18.1
-GTTAC**TGTGGGAA**AGAAAG-	100	$1.06\ (\pm0.1) \times 10^7$	94	−8.94	8.62 (±0.1)	−17.5
	125	$1.27\ (\pm0.3) \times 10^7$	79	−9.04	8.27 (±0.1)	−17.3
	150	$7.78\ (\pm0.8) \times 10^6$	129	−8.76 (±0.1)	9.18 (±0.3)	−17.9 (±0.3)
	175	$2.00\ (\pm0.2) \times 10^6$	500	−8.01	7.99 (±0.08)	−16.0
	200	$3.79\ (\pm0.5) \times 10^5$	2,639	−7.09	7.44 (±0.3)	−14.5
Nonconsensus	50	$1.40\ (\pm0.8) \times 10^7$	71	−9.09	7.01 (±0.3)	−16.1
-CGGCT**CGTGTGAA**ACTTCC-	100	$6.97\ (\pm1.5) \times 10^6$	143	−8.70	6.34 (±0.1)	−15.0
	125	$1.11\ (\pm0.3) \times 10^7$	90	−8.96	5.92 (±0.1)	−14.9
	150	$3.45\ (\pm0.9) \times 10^6$	307	−8.30 (±0.2)	6.54 (±0.8)	−14.8 (±0.6)
	175	$2.63\ (\pm0.6) \times 10^6$	380	−8.17	4.97 (±0.2)	−13.1
	200	$3.19\ (\pm0.5) \times 10^5$	3,135	−7.00	4.70 (±0.3)	−11.7

All experiments are performed at 5°C.
For all experiments, the errors represent the standard deviation of the nonlinear least squares fit of the data to the titration curves, except for binding experiments performed at 150 mM, where the data values and errors are taken from Table I.

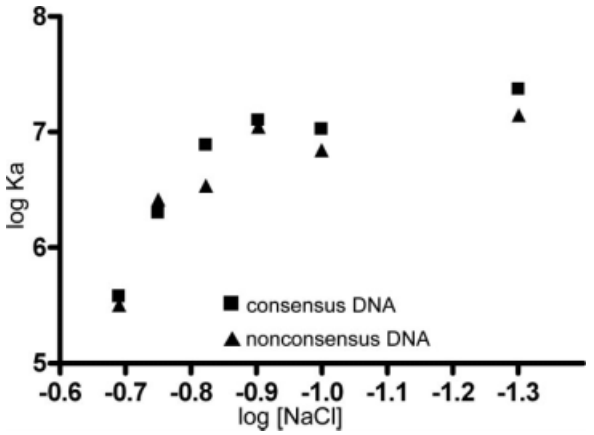

Figure 4. Salt dependence of CSL binding to DNA. Figure shows the plot of log K_a (association constant) versus the log of NaCl concentration for CSL binding to the *HES-1* consensus DNA site (■) and nonconsensus DNA site (▲). Binding experiments were performed at 50, 100, 125, 150, 175, and 200 m*M* NaCl.

deviation (RMSD) of 1.1 Å. Alignments of individual domains of CSL (NTD, BTD, and CTD) display higher degrees of correspondence, with RMSDs of 0.27, 0.29, and 0.20 Å for overlays of NTD, BTD, and CTD, respectively; however, there are moderate differences in the relative arrangement of domains, as overlaying the NTD from the consensus and nonconsensus structures reveals shifts of 4–5 Å in the corresponding positions for the Cα atoms in the BTD and CTD.

Comparison of the protein-DNA interfaces between the two complex structures also reveals a high degree of similarity. The interface formed between CSL and the consensus and nonconsensus DNA sites buries 1,070 $Å^2$ and 1,046 $Å^2$ of surface area, respectively.[35] The similarity in BSA between the two complexes is entirely consistent with the nearly identical ΔCp values determined earlier. Moreover, essentially all of the nonspecific and specific protein-DNA contacts that are observed in the CSL-consensus DNA complex are maintained in the CSL-nonconsensus DNA complex. In addition, the number of water molecules bound at the protein-DNA interface is similar for the two complexes. Overall, the backbone conformations of the two DNA duplexes are also similar with moderate differences observed for the DNA base parameters. Overlaying the corresponding phosphorus atoms from the phosphodiester backbone of the two DNA duplexes results in a 0.77 Å RMSD, with greater structural correspondence observed between aligning the top single DNA strands (-ACTGTGGGAAAGA- vs. -ATCGTGTGAAAGA-) over the bottom single strands (-TCTTTCCCACAGT- vs. -TCTTTCACACGAT-). Analysis of the T/A base step in the nonconsensus duplex (-CGTG**T**GAA-) reveals neither any large perturbations in the conformation of the DNA bases or backbone nor any changes in the protein. However, the nonconsensus DNA structure displays a much higher degree of propeller twist than the consensus DNA duplex (Supporting Information Table S2). The average propeller twist for base steps of typical B-DNA is ±10°[36]; the consensus and nonconsensus DNA sites have average propeller twists of −11 and −14, respectively. Moreover, base pairs upstream and downstream of the T/A base step in the nonconsensus DNA duplex have elevated propeller twists values, ranging from −17° to −20°. In addition, a modest 2 Å decrease in the width of the minor groove upstream of the T/A base step is observed for the nonconsensus site, when compared with the consensus site, with a compensatory increase of the major groove width downstream of the T/A base step.

We next examined and compared other regions of the consensus and nonconsensus DNA complexes with CSL, which revealed three other notable structural differences between the complexes: first, a β-hairpin loop in the BTD, which makes contacts in the minor groove of DNA, assumes an alternate conformation in the consensus complex, but not the nonconsensus DNA; second, a large loop structure in the BTD, which binds the RAM domain of NotchIC, is completely ordered in the nonconsensus complex, but largely disordered in the consensus complex;

Table IV. *pH Dependence of CSL Binding to Consensus and Nonconsensus HES-1 sites*

	pH	K_{app} (M^{-1})	K_d (n*M*)	ΔG_{obs} (kcal/mol)	ΔH_{obs} (kcal/mol)	$-T\Delta S_{obs}$ (kcal/mol)
Consensus	6.0	$1.56\ (\pm0.3) \times 10^7$	64	−9.15	9.11 (±0.1)	−18.3
-GTTAC**TGTGGGAA**AGAAAG-	6.5	$8.04\ (\pm2.3) \times 10^6$	124	−8.78	9.14 (±0.3)	−17.9
	7.0	$2.73\ (\pm0.4) \times 10^6$	366	−8.19	5.40 (±0.09)	−13.6
	7.5	$2.22\ (\pm0.4) \times 10^6$	450	−8.07	6.86 (±0.2)	−14.9
	8.0	$1.13\ (\pm0.2) \times 10^6$	885	−7.70	6.99 (±0.2)	−14.7
Nonconsensus	6.0	$1.53\ (\pm0.6) \times 10^7$	65	−9.14	5.41 (±0.2)	−14.5
-CGGCT**CGTGTGAA**ACTTCC-	6.5	$3.80\ (\pm0.9) \times 10^6$	263	−8.37	6.17 (±0.2)	−14.5
	7.0	$1.63\ (\pm0.3) \times 10^6$	613	−7.90	6.74 (±0.2)	−14.6
	7.5	$1.13\ (\pm0.3) \times 10^6$	885	−7.70	4.60 (±0.4)	−12.3
	8.0	$9.16\ (\pm1.5) \times 10^5$	1092	−7.58	3.99 (±0.2)	−11.6

All experiments are performed at 5°C.
The errors represent the standard deviation of the nonlinear least squares fit of the data to the titration curves.

Table V. *Thermodynamic Data for CSL Binding to the HES-1 Nonconsensus Site With Either T→A or T→C Base Pair Substitutions*

DNA	K (M^{-1})	K_d (nM)	ΔG° (kcal/mol)	ΔH° (kcal/mol)	−TΔS° (kcal/mol)
T→A mutation	5.98 (±1.1) × 10^6	170	−8.7 (±0.1)	6.0 (±0.4)	−14.6 (±0.4)
T→C mutation	9.97 (±0.5) × 10^5	1,003	−7.6 (±0.02)	6.3 (±0.9)	−13.9 (±0.9)

T→A mutation DNA, -CGGCTCGTG**A**GAAACTTCC-; T→C mutation DNA, -CGGCTCGTG**C**GAAACTTCC-.
All experiments are performed at 5°C.
Values are the mean of at least two independent experiments, and the errors represent the standard deviation of multiple experiments.

and third, a loop in the NTD (termed the NTD-loop), which adopts an open conformation when CSL binds Mastermind, is in an open conformation in the nonconsensus complex, but in a closed conformation in the consensus complex.

In previous CSL structures, it was shown that the BTD recognizes the first two base steps of the consensus binding site (-**TG**TGGGAA-) via a β-hairpin loop structure that inserts into the minor groove, making nonspecific and specific contacts with the

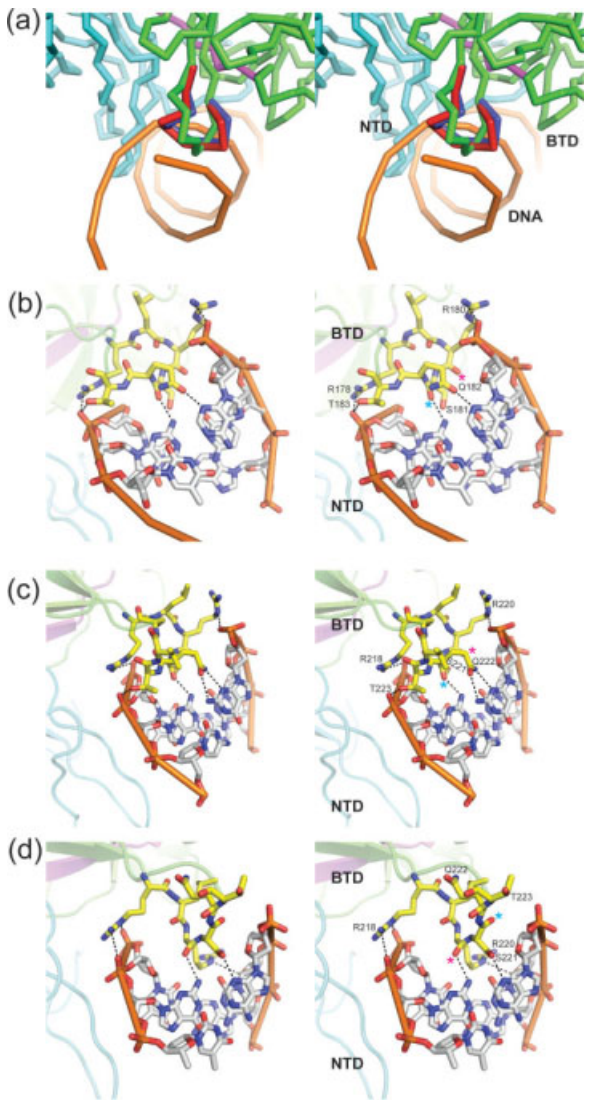

Figure 5. BTD-DNA interactions. Figure shows the structural details of the BTD interaction with DNA and highlights the conformational differences in a β-hairpin loop motif between structures. Wall-eye stereo pairs are depicted. (A) Simplified overview of interactions between the BTD of CSL and DNA, showing the insertion of the β-hairpin loop motif into the minor groove of DNA. The cα trace for the NTD and BTD of CSL are colored cyan and green, respectively. The DNA backbone is represented as a ribbon and colored orange. The β-hairpin loop motifs from the murine CSL consensus DNA structure (3BRG), the human ternary complex structure (2F8X), and the murine CSL nonconsensus DNA structure (3IAG) are colored green, red, and blue, respectively. Note the high degree of structural correspondence between 2F8X (red) and 3IAG (blue), but the large structural change in the β-hairpin loop motif for 3BRG (green). (B) Zoom view of the BTD interaction with DNA from the human CSL-NotchIC-Mastermind ternary complex structure (2F8X). The β-hairpin loop is in a stick representation with standard coloring for the atoms (yellow, red, and blue for carbon, oxygen, and nitrogen atoms, respectively). The DNA is also in a stick representation and colored grey, red, blue, and orange for carbon, oxygen, nitrogen, and phosphorous atoms, respectively. For clarity, only three base pairs of the DNA are shown (-**TGT**GGGAA-). Hydrogen bonds are indicated with black dashed lines. As also observed in previous CSL structures (e.g., 1TTU and 2FO1), Q182 makes hydrogen-bonding interactions with the adenine in the first T/A base step and the backbone carbonyl of S181 (denoted with a cyan asterisk) makes hydrogen-bonding interactions with the guanine at the following G/C base step. Nonspecific interactions with the DNA backbone mediated by residues R178, R180, and T183 are also shown, and the backbone carbonyl of R180 is indicated with a magenta asterisk. (C) Corresponding zoom view of murine CSL nonconsensus DNA complex structure determined here (3IAG). Orthologous residues and hydrogen bonding pattern are depicted, demonstrating identical interactions as described earlier. (d) Zoom view of murine CSL consensus DNA complex structure (3BRG), highlighting structural rearrangement of β-hairpin loop. In this conformation of the BTD loop, the side chains of Q222 and T223 and the backbone carbonyl of S221 no longer form interactions with the DNA; however, the rearrangement allows the side chain of S221 to make hydrogen-bonding interactions with the adenine in the T/A base step (-**T**GTGGGAA-) and the backbone carbonyl of R220 to make hydrogen-bonding interactions with the guanine in the G/C base step (-T**G**TGGGAA-). Thus, despite the rearrangement, equivalent interactions with the DNA are maintained.

DNA [Fig. 5(A)].[17] These structures revealed that the side chain of an absolutely conserved glutamine residue and the backbone carbonyl of an absolutely conserved serine residue make hydrogen bonding interactions with the purine bases of the T/A and G/C base steps, respectively [Fig. 5(B)]. As shown in Figure 5(C), despite the T/A to C/G base pair change at this position, similar interactions are maintained for CSL binding to the nonconsensus site (-**CG**TGTGAA-). However, for the mouse CSL consensus structure, the conformation of the β-hairpin loop substantially deviates from previous structures [Figure 5(A,D)]. In this structure, the glutamine side chain (Gln222) repositions itself into an orientation that points away from the DNA, eliminating any interactions with the T/A base step [Fig. 5(D)]. Interestingly, new BTD-DNA contacts are made in the minor groove that maintain specificity—the side chain of Ser221 moves into the space vacated by Gln222, making equivalent hydrogen bonding interactions with the T/A base step, and the backbone carbonyl of Arg220 makes equivalent interactions with the G/C base step [Fig. 5(D)]. Thus, despite the dramatic structural rearrangement, equivalent specific and nonspecific interactions with the DNA are maintained.

The second notable structural difference between the consensus and nonconsensus CSL-DNA structures occurs within a large loop structure of the BTD, which functions in binding the RAM domain of NotchIC. Previous structures have shown that in the absence of RAM or other bound coregulators, this BTD loop is largely disordered.[17,20] This is the case for the previously determined mouse CSL-consensus DNA structure—the residues 256–261 were not modeled in the structure due to a lack of interpretable electron density for this region; however, in the mouse, CSL-nonconsensus DNA structure determined here this RAM binding loop of the BTD is completely resolved, albeit with elevated B-factors, forming a comparable structure to what is observed for CSL-RAM structures and CSL-NotchIC-Mastermind ternary complex structures. We attempted to remodel and refine the disordered BTD loop from the CSL-consensus DNA complex, using the ordered BTD loop structure from the nonconsensus CSL-DNA complex. Although the refinement was successful, no appreciable or significant additional electron density was observed for the BTD loop in the CSL-consensus DNA complex. Moreover, the side chain of Arg264, which is ordered in both structures and makes protein contacts at the *C*-terminal end of the BTD loop, is in two different, but well-defined conformations. Taken together, these data suggest that the BTD loop forms two distinct structural elements in the two complexes and supports our original decision not to model this loop in the CSL-consensus DNA structure.

The final structural difference of note is observed within the NTD of CSL, regarding a β-hairpin loop structure that is involved in Mastermind binding and termed the NTD-loop. In CSL structures complexed with NotchIC and Mastermind, that is, a transcriptionally active complex, the NTD-loop is an open conformation to accommodate binding of the *C*-terminal helical region of Mastermind.[18,19] In structures of CSL without bound coregulators, the NTD-loop is in a closed conformation[17,20]; in structures of CSL bound to the RAM domain of NotchIC, the loop is also in an open conformation.[20] These data have in part led to an allosteric model, in which RAM binding to the BTD triggers opening of the NTD-loop, to facilitate Mastermind binding and ternary complex formation. In the previously determined mouse CSL-consensus DNA structure, the NTD-loop was observed in a closed conformation. In the CSL-nonconsensus DNA structure determined here, the NTD-loop adopts a more open conformation, with the caveat that the B-factors are greatly elevated for the main chain atoms in this region—over the residue range Ile131 to Glu137, the average Cα B-factor is 54 and 37 for the nonconsensus and consensus DNA complexes with CSL, respectively. The potentially correlative conformations of the BTD-RAM binding loop and the NTD-loop are discussed later.

Discussion

The ability of CSL to specifically recognize and bind DNA sites within the promoter regions of Notch responsive genes *in vivo* is one of the fundamental aspects to understanding how transcription is regulated in the pathway. Despite this simple axiom, very little is understood at the quantitative level regarding the affinity of CSL for DNA. In fact, to our knowledge, only one early study in the field has attempted to determine the dissociation constant (K_d) for CSL binding to DNA. In this previous study, a K_d of 1 n*M* was estimated from Scatchard plot analyses of CSL-DNA electrophoretic mobility shift assay (EMSAs), using CSL (*aka* RBP-Jκ) protein that was partially purified from nuclear extracts.[37] Despite the caveats associated with these types of experiments and data analysis, the apparent high affinity of CSL for DNA, in conjunction with subsequent studies that demonstrated CSL functions as both an activator and repressor, has led to current models in the field that suggest CSL is statically bound to DNA while regulating transcription from Notch target genes. However, more recent studies suggest that CSL binding to DNA is a dynamic rather than static process, and that recruitment of CSL, via cooperative interactions, to target genes is an important mechanism of regulation.[22,38,39] Taken together, these studies imply our understanding of

CSL-DNA interactions, and the role these play in transcriptional regulation are incomplete.

The focus of our studies were 2-fold; first, we wanted to provide a quantitative and comprehensive characterization of the energetics that underlie CSL-DNA binding, thereby providing a baseline for understanding the assembly of Notch transcription complexes at more complicated DNA elements, such as the *HES-1* SPS. For these studies, we used highly purified recombinant preparations of CSL and chose to analyze individually the two CSL binding sites that compose the *HES-1* SPS, as this would provide binding data for CSL interacting with both a consensus and nonconsensus binding site. Second, we wanted to provide additional structural information for CSL interacting with DNA sites other than the 5′ consensus site from the *HES-1* SPS, because all CSL-DNA complex structures determined to date have used the same DNA binding site.

Our binding studies demonstrate that CSL has only moderate affinity for DNA with dissociation constants of at least 100 and 250 n*M* for the *HES-1* consensus and nonconsensus DNA sites, respectively (Table I). This represents at least 100-fold weaker affinity for DNA than what was previously reported. Moreover, the observed trends in binding were conserved in worm and fly CSL orthologs (Table II), suggesting that the moderate affinity of CSL for DNA is a universal aspect of Notch signaling in all organisms. In contrast, under identical experimental conditions, we previously determined that the RAM domain of NotchIC from mouse has an approximately 3- to 8-fold higher affinity for CSL than what was determined here for CSL-DNA complexes. For comparison, we also determined the DNA affinity for a structurally related transcription factor—the p50 homodimer, a repressor in the NF-kappaB signaling pathway—binding to the Ig-κB DNA site (Supporting Information Fig. S3). In contrast to CSL, p50 binding to DNA was very sensitive to temperature with >30-fold higher affinity observed at 30°C than binding experiments performed at 10°C; nonetheless, over the temperature range tested, p50 in general, has a similarly modest affinity for DNA, suggesting that both CSL, and p50 binding to DNA may be modulated by interactions with neighboring transcription factors. Two other points should also be mentioned, first, our experimentally determined values for the affinity of p50 for DNA by ITC are very similar to the values previously reported using gel-shift and fluorescence anisotropy binding assays[30]; and second, the moderate affinity of CSL for DNA we determined here is not an artifact of our experimental setup; as shown in Table S3, a number of transcription factors with low nanomolar dissociation constants for DNA have been characterized using ITC. Taken together, the modest affinity of CSL for DNA suggests that not all CSL binding sites *in vivo* are occupied at all times and that CSL-coregulator complexes are likely forming/exchanging in the nucleoplasm and on DNA, which in our mind, places much more emphasis on cooperative mechanisms that recruit CSL to sites on the DNA than previously appreciated.

Our comparative analyses of CSL binding the 5′ consensus and 3′ nonconsensus sites of the *HES-1* SPS revealed only minor differences in the affinity and overall free energy for the two complexes. In both cases, the binding reaction is entropically driven, relatively insensitive to temperature, and endothermic at the temperatures tested (5°C–15°C); however, the differences in binding are significantly larger than the error in the measurements and the entropic/enthalpic contributions to the overall free energy of binding are distinctly different for the two complexes (Table I). This suggests that the two DNA binding sites, at least at the thermodynamic level, are not identical in the complexes they form with CSL. Additional comparisons, as a function of temperature, salt, and pH, did not reveal any further differences between the consensus and nonconsensus sites. In both cases, binding was very sensitive to the concentration of salt (Table III), suggesting that ionic interactions contribute largely to binding; this is consistent with the entropically favorable release of counterions underlying complex formation. Interestingly, a similar strong dependence on salt concentration is observed for the p50/p65 NF-κB heterodimer.[30] Under the experimental conditions tested, CSL binding to both sites was linearly dependent on pH, with the tightest binding observed at pH 6.0. Although a binding study over a broader pH range would be more definitive, nevertheless these data potentially indicate that one ionizable protein residue with a pKa in the range of 6.0 to 8.0, possibly a cysteine or histidine residue, plays a role in CSL-DNA binding.[34] However, if this were the case, there is neither a histidine nor a cysteine residue located at the protein-DNA interface that would readily explain the pH dependence of binding.

Given the small differences in affinity that we observed for CSL binding the 5′ consensus and 3′ nonconsensus sites of the HES1 SPS, we were curious as to why previous studies that identified the consensus binding site for CSL revealed a strong preference for a G/C base step at this position (-C/tGTG**G**GAA-), as opposed to A/T, C/G, and T/A base steps. Previous structures have shown that in some, but not all CSL-DNA complexes, the side chain of an absolutely conserved glutamine residue makes a water-mediated contact with the guanine base in the major groove, providing some explanation for the specificity and tolerance for purine bases at this position.[17] Despite these structural results, there is relatively strong conservation for a T/A base step, that is, pyrimidine base, at this position in the *HES-1* SPS found in mammals,

Xenopus, and Zebrafish. Although the T→A mutation of the nonconsensus site (-CGTG**T**GAA-) actually enhanced binding similar to the consensus site, strikingly, the T→C mutation had a profound reduction in binding. Taken together, these results suggest that the identity of this base step is important for the affinity and specificity of CSL binding; however, a satisfactory molecular explanation for the observed differences in binding are still lacking.

With the exception of a β-hairpin loop structure in the BTD that participates in DNA binding, which will be discussed in greater detail later, our comparison of the CSL-nonconsensus DNA structure determined here with the previously determined CSL-consensus DNA structure revealed no overtly conspicuous structural differences between the protein-DNA contacts between the two complexes; the amounts of BSA at the protein-DNA interface were similar; the number of specific and nonspecific DNA interactions were similar; and, the number of water molecules bound at the protein-DNA interface were also similar. Thus, overall our structural studies are consistent with our binding studies. However, on closer examination, we noticed that the base pairs in the nonconsensus DNA duplex had a much higher degree of propeller twist than for the corresponding regions in the consensus DNA duplex (Table S2). In fact, certain base steps in the nonconsensus DNA duplex had propeller twists that were far outside the values typically observed for B-DNA. We believe that the higher degree of propeller twist observed in the CSL-nonconsensus DNA complex may account for two observations from our binding data: (1) if the binding of CSL to the nonconsensus DNA induces the unfavorable propeller twist observed in this complex, then this would likely decrease the overall free energy (ΔG°) of complex formation, which is consistent with our binding data (Table I); and (2) if the greater propeller twist observed in the nonconsensus DNA allows for increased hydrogen bonding interactions between consecutive base steps in duplex,[36] then this could account for the more favorable enthalpic contribution to binding observed for the CSL-nonconsensus DNA complex (Table I).

Additional comparisons of the two complexes did reveal a striking conformational difference in the CSL-consensus DNA structure for a β-hairpin loop located within the BTD of CSL (Fig. 5). This β-hairpin loop contributes to DNA binding via nonspecific and specific contacts mediated through the minor groove of DNA. Despite the dramatic rearrangement of a glutamine residue within this loop, which contributes specific DNA contacts in all other CSL-DNA structures, the new side chain and backbone interactions that are formed maintain equivalent nonspecific and specific interactions with the DNA. Thus, we do not expect that these structural changes account for any of the differences in affinity we observed in our consensus and nonconsensus binding studies with CSL. Interestingly, an analogous structural rearrangement occurs within one of the previous CSL-RAM-DNA complex structures we determined with Notch components from *C. elegans* (PDB ID: 3BRF).[20] We believe these structures reveal a novel mode of DNA binding mediated by the BTD of CSL, highlighting an additional level of plasticity in DNA recognition, which likely accounts for the less stringent requirements for base pairs in this region of the consensus binding site.

Finally, structural comparisons of the two CSL-DNA complexes revealed additional molecular details regarding the dynamic interplay between a large loop structural element in the BTD, which is critical for binding the RAM domain of NotchIC, and the NTD-loop, which is important for binding the *C*-terminal helix of Mastermind. In the previous CSL-consensus DNA structure, the BTD-RAM binding loop is disordered, with minimal interpretable electron density associated with it, and the NTD-loop is in a closed conformation[20]; in the CSL-nonconsensus DNA structure determined here, the BTD-RAM binding loop is completely ordered, with continuous electron density, and the NTD-loop is in more of an open conformation, but with significantly elevated B-factors. It is interesting to note that in all previous CSL-coregulator structures (human and worm CSL-NotchIC-Mastermind ternary complexes, and worm CSL-RAM complexes) when the BTD-RAM binding loop forms an ordered structure, the NTD-loop is in an open conformation. These data suggest that opening and closing of the BTD-RAM binding loop affects whether the NTD-loop is an open or closed conformation, that is, ordering of the BTD-RAM binding loop either intrinsically or through binding the RAM domain of NotchIC allosterically induces the opening of the NTD-loop, which is required for Mastermind binding and formation of the active ternary complex. Intriguingly, Arg226, which resides at the *C*-terminal end of the BTD-RAM binding loop, may be serving as a hinge or switch residue, as its side chain assumes two distinct conformations in the two complexes, seemingly dependent on whether the BTD-RAM binding loop forms an ordered or disordered structural element.

Materials and Methods

Cloning, expression, and protein purification

The cloning, expression, and purification of *C. elegans* and *M. musculus* CSL recombinant proteins from bacteria were described previously.[20,17]

Oligomeric DNA duplexes for ITC binding studies

The following 19-mer oligomeric DNA duplexes that correspond to the 5′ consensus and 3′ nonconsensus

sites of the *HES-1* SPS were purchased from Operon Biotechnologies; consensus: 5′-CGGCC**TGTGGGAA**ACTTCC-3′, 5′-GGAAGT**TTCCCACA**GGCCG-3′; nonconsensus: 5′-CGGCT**CGTGTGAA**ACTTCC-3′, 5′-GGAAGT**TTCACAC**GAGCCG-3′.Single-stranded DNA oligos were resuspended in a buffer containing 10 m*M* Tris 8.0, 500 m*M* NaCl, and 1 m*M* $MgCl_2$, quantitated spectroscopically at A_{260}, mixed equimolar with the complimentary oligo, boiled for 10 min, and allowed to slow cool at room temperature to ensure optimal duplex annealing. Size exclusion chromatography was used to purify 19-mer DNA duplexes and buffer match DNA samples for ITC binding experiments. Samples were validated for CSL binding via EMSA and were quantified by ultraviolet absorbance measurements at 260 nm.

Isothermal titration calorimetry

ITC experiments were performed using a Microcal VP-ITC micocalorimeter. For all binding reactions, approximately 100 μ*M* DNA was loaded into the syringe and titrated into 10 μ*M* CSL in the cell. The c value ($c = K_a[M]N$) for all experiments ranged between 3 and 250. ITC binding experiments were performed in 50 m*M* sodium phosphate pH 6.5, 150 m*M* NaCl at 5°C, 10°C, or 15°C; experiments performed at 20°C, 25°C, 37°C, or 45°C yielded no measurable heat associated with binding. The salt dependence of binding experiments was performed in 50 m*M* sodium phosphate pH 6.5, and 50, 100, 125, 150, 175, or 200 m*M* NaCl. pH-dependent experiments were performed in 50 m*M* sodium phosphate, pH 6.0, 6.5, 7.0, 7.5, or 8.0, and 150 m*M* NaCl. The collected data were analyzed using the ORIGIN software and fit to a one site binding model with an average N (ligand/macromolecule) value of 0.93 and 0.92 for CSL binding the consensus and nonconsensus DNA, respectively.

Crystallization and data collection

A 13-mer DNA duplex with single-stranded TT/AA overhangs corresponding to the 3′ nonconsensus site from the *HES-1* SPS was cocrystallized with mouse CSL. CSL-DNA complexes were set up in a 1:1.1 molar ratio and screened for crystallization conditions using the Hampton Research Index Screen and an Art Robbins Phoenix Crystallization Robot. The final optimized crystallization conditions were in a mother liquor containing 100 m*M* magnesium formate and 19% polyethylene glycol 3350 at 4°C. Crystals were cryoprotected in mother liquor solutions containing 20% xylitol and flash frozen in LN2. The diffraction data were collected at the Advanced Photon Source, beamline 22-ID. The crystals diffracted to 2.0 Å and belong to the orthorhombic space group $P2_12_12$, with unit cell dimensions a = 63.45Å, b = 93.14Å, and c = 112.50Å (Supporting Information Table S1).

Structure determination, model building, and refinement

The structure of mouse CSL bound to DNA (3BRG), corresponding to the 5′ consensus site of the *HES-1* SPS, was used with Phaser to obtain a molecular replacement solution for our mouse CSL-nonconsensus DNA diffraction data.[40] Prime-and-switch phasing from RESOLVE was used to decrease model bias, and Coot was used to rebuild missing parts of the model.[41,42] translation/libration/screw (TLS) parameters were generated and used for refinement in Refmac.[43,44] The structure was validated with PROCHECK and Molprobity.[45,46] The final model of CSL consisted of amino acids 53–474, and the entire DNA duplex. The structure has been refined to an $R_{work} = 20.0\%$ and $R_{free} = 24.4\%$ with good geometry (Supporting Information Table S1) and deposited in the Protein Data Bank. Pymol was used to align structures and to create Figure 5 (pymol.sourceforge.net). The PISA server was used to analyze protein-DNA interfaces.[35] Coordinates and structure factors have been deposited in the Protein Data Bank with accession number 3IAG.

Acknowledgments

We thank Zhenyu Yuan and other members of the Kovall Laboratory for their assistance with protein purification and data collection. We also thank Andrew Herr for his insightful discussions regarding our binding data and the beamline staff at the Advanced Photon Source SER-CAT 22-ID.

References

1. Artavanis-Tsakonas S, Rand MD, Lake RJ (1999) Notch signaling: cell fate control and signal integration in development. Science 284:770–776.
2. Tanigaki K, Honjo T (2007) Regulation of lymphocyte development by Notch signaling. Nat Immunol 8: 451–456.
3. Gridley T (2003) Notch signaling and inherited disease syndromes. Hum Mol Genet 12:R9–R13.
4. High FA, Epstein JA (2008) The multifaceted role of Notch in cardiac development and disease. Nat Rev Genet 9:49–61.
5. Aster JC, Pear WS, Blacklow SC (2008) Notch signaling in leukemia. Annu Rev Pathol 3:587–613.
6. Kopan R, Ilagan MX (2009) The canonical Notch signaling pathway: unfolding the activation mechanism. Cell 137:216–233.
7. Bray SJ (2006) Notch signalling: a simple pathway becomes complex. Nat Rev Mol Cell Biol 7:678–689.
8. Tun T, Hamaguchi Y, Matsunami N, Furukawa T, Honjo T, Kawaichi M (1994) Recognition sequence of a highly conserved DNA binding protein RBP-J kappa. Nucl Acids Res 22:965–971.
9. Meng X, Brodsky MH, Wolfe SA (2005) A bacterial one-hybrid system for determining the DNA-binding specificity of transcription factors. Nat Biotechnol 23: 988–994.
10. Brou C, Logeat F, Lecourtois M, Vandekerckhove J, Kourilsky P, Schweisguth F, Israel A (1994) Inhibition of the DNA-binding activity of *Drosophila* suppressor

of hairless and of its human homolog, KBF2/RBP-J kappa, by direct protein-protein interaction with *Drosophila* hairless. Genes Dev 8:2491–2503.
11. Christensen S, Kodoyianni V, Bosenberg M, Friedman L, Kimble J (1996) lag-1, a gene required for lin-12 and glp-1 signaling in *Caenorhabditis elegans*, is homologous to human CBF1 and *Drosophila* Su(H). Development 122:1373–1383.
12. Bailey AM, Posakony JW (1995) Suppressor of hairless directly activates transcription of enhancer of split complex genes in response to Notch receptor activity. Genes Dev 9:2609–2622.
13. Yoo AS, Bais C, Greenwald I (2004) Crosstalk between the EGFR and LIN-12/Notch pathways in *C. elegans* vulval development. Science 303:663–666.
14. Ling PD, Rawlins DR, Hayward SD (1993) The Epstein-Barr virus immortalizing protein EBNA-2 is targeted to DNA by a cellular enhancer-binding protein. Proc Natl Acad Sci USA 90:9237–9241.
15. Liang Y, Chang J, Lynch SJ, Lukac DM, Ganem D (2002) The lytic switch protein of KSHV activates gene expression via functional interaction with RBP-Jkappa (CSL), the target of the Notch signaling pathway. Genes Dev 16:1977–1989.
16. Jarriault S, Brou C, Logeat F, Schroeter EH, Kopan R, Israel A (1995) Signalling downstream of activated mammalian Notch. Nature 377:355–358.
17. Kovall RA, Hendrickson WA (2004) Crystal structure of the nuclear effector of Notch signaling, CSL, bound to DNA. EMBO J 23:3441–3451.
18. Wilson JJ, Kovall RA (2006) Crystal structure of the CSL-Notch-mastermind ternary complex bound to DNA. Cell 124:985–996.
19. Nam Y, Sliz P, Song L, Aster JC, Blacklow SC (2006) Structural basis for cooperativity in recruitment of MAML coactivators to Notch transcription complexes. Cell 124:973–983.
20. Friedmann DR, Wilson JJ, Kovall RA (2008) RAM-induced allostery facilitates assembly of a notch pathway active transcription complex. J Biol Chem 283: 14781–14791.
21. Kovall RA (2007) Structures of CSL, Notch and Mastermind proteins: piecing together an active transcription complex. Curr Opin Struct Biol 17:117–127.
22. Nam Y, Sliz P, Pear WS, Aster JC, Blacklow SC (2007) Cooperative assembly of higher-order Notch complexes functions as a switch to induce transcription. Proc Natl Acad Sci USA 104:2103–2108.
23. Lundback T, Hard T (1996) Sequence-specific DNA-binding dominated by dehydration. Proc Natl Acad Sci USA 93:4754–4759.
24. Merabet E, Ackers GK (1995) Calorimetric analysis of lambda cI repressor binding to DNA operator sites. Biochemistry 34:8554–8563.
25. Sturtevant JM (1977) Heat capacity and entropy changes in processes involving proteins. Proc Natl Acad Sci USA 74:2236–2240.
26. Livingstone JR, Spolar RS, Record MT, Jr (1991) Contribution to the thermodynamics of protein folding from the reduction in water-accessible nonpolar surface area. Biochemistry 30:4237–4244.
27. Spolar RS, Record MT, Jr (1994) Coupling of local folding to site-specific binding of proteins to DNA. Science 263:777–784.
28. Spolar RS, Livingstone JR, Record MT, Jr (1993) Use of liquid hydrocarbon and amide transfer data to estimate contributions to thermodynamic functions of protein folding from the removal of nonpolar and polar surface from water. Biochemistry 31:3947–3955.
29. Jin L, Yang J, Carey J (1993) Thermodynamics of ligand binding to trp repressor. Biochemistry 32: 7302–7309.
30. Phelps CB, Sengchanthalangsy LL, Malek S, Ghosh G (2000) Mechanism of kappa B DNA binding by Rel/NF-kappa B dimers. J Biol Chem 275:24392–24399.
31. Villemain JL, Giedroc DP (1996) Characterization of a cooperativity domain mutant Lys3 –> Ala (K3A) T4 gene 32 protein. J Biol Chem 271:27623–27629.
32. Ha JH, Capp MW, Hohenwalter MD, Baskerville M, Record MT, Jr (1992) Thermodynamic stoichiometries of participation of water, cations and anions in specific and non-specific binding of lac repressor to DNA. Possible thermodynamic origins of the "glutamate effect" on protein-DNA interactions. J Mol Biol 228:252–264.
33. Lohman TM, Mascotti DP (1992) Thermodynamics of ligand-nucleic acid interactions. Methods Enzymol 212: 400–424.
34. Wyman J, Gill SJ (1990) Binding and linkage: functional chemistry of biological macromolecules. Mill Valley, California: University Science Books, xiii, 330 p.
35. Krissinel E, Henrick K (2007) Inference of macromolecular assemblies from crystalline state. J Mol Biol 372: 774–797.
36. el Hassan MA, Calladine CR (1996) Propeller-twisting of base-pairs and the conformational mobility of dinucleotide steps in DNA. J Mol Biol 259:95–103.
37. Hamaguchi Y, Matsunami N, Yamamoto Y, Honjo T (1989) Purification and characterization of a protein that binds to the recombination signal sequence of the immunoglobulin J kappa segment. Nucleic Acids Res 17:9015–9026.
38. Krejci A, Bray S (2007) Notch activation stimulates transient and selective binding of Su(H)/CSL to target enhancers. Genes Dev 21:1322–1327.
39. Neves A, English K, Priess JR (2007) Notch-GATA synergy promotes endoderm-specific expression of ref-1 in *C. elegans*. Development 134:4459–4468.
40. Read RJ (2001) Pushing the boundaries of molecular replacement with maximum likelihood. Acta Cryst D57:1373–1382.
41. Terwilliger TC (2000) Maximum-likelihood density modification. Acta Cryst D56:965–972.
42. Emsley P, Cowtan K (2004) Coot: model-building tools for molecular graphics. Acta Cryst D60:2126–2132.
43. Winn MD, Isupov MN, Murshudov GN (2001) Use of TLS parameters to model anisotropic displacements in macromolecular refinement. Acta Cryst D57:122–133.
44. Murshudov GN, Vagin AA, Dodson EJ (1997) Refinement of macromolecular structures by the maximum-likelihood method. Acta Cryst D53:240–255.
45. Laskowski RA, Moss DS, Thornton JM (1993) Main-chain bond lengths and bond angles in protein structures. J Mol Biol 231:1049–1067.
46. Davis IW, Leaver-Fay A, Chen VB, Block JN, Kapral GJ, Wang X, Murray LW, Arendall WB, III, Snoeyink J, Richardson JS, Richardson DC (2007) MolProbity: all-atom contacts and structure validation for proteins and nucleic acids. Nucl Acids Res 35:W375–W383.